Crystal structure of rat heme oxygenase-1 in complex with heme

Masakazu Sugishima[a,1], Yoshiaki Omata[b,1], Yoshimitsu Kakuta[a], Hiroshi Sakamoto[b], Masato Noguchi[b], Keiichi Fukuyama[a,*]

[a] *Department of Biology, Graduate School of Science, Osaka University, Toyonaka, Osaka 560-0043, Japan*
[b] *Department of Medical Biochemistry, Kurume University School of Medicine, 67 Asahi-machi, Kurume 830-0011, Japan*

Received 10 February 2000

Edited by Hans Eklund

Abstract Heme oxygenase catalyzes the oxidative cleavage of protoheme to biliverdin, the first step of heme metabolism utilizing O_2 and NADPH. We determined the crystal structures of rat heme oxygenase-1 (HO-1)–heme and selenomethionyl HO-1–heme complexes. Heme is sandwiched between two helices with the δ-*meso* edge of the heme being exposed to the surface. Gly143N forms a hydrogen bond to the distal ligand of heme, OH^-. The distance between Gly143N and the ligand is shorter than that in the human HO-1–heme complex. This difference may be related to a pH-dependent change of the distal ligand of heme. Flexibility of the distal helix may control the stability of the coordination of the distal ligand to heme iron. The possible role of Gly143 in the heme oxygenase reaction is discussed.

Key words: Heme oxygenase; Heme metabolism; Redox reaction; Enzyme–substrate complex; X-ray crystallography

1. Introduction

Heme oxygenase (HO, EC 1.14.99.3), a microsomal enzyme which oxidizes protoheme to biliverdin IXα, plays a key role in physiological heme metabolism. The first step of heme degradation catalyzed by HO is the oxidation of heme to α-hydroxyheme requiring O_2 and reducing equivalents from NADPH cytochrome P450 reductase [1,2]. The second step is the formation of verdoheme with concomitant release of hydroxylated α-*meso* carbon as carbon monoxide [3–5]. It is suggested that CO serves as a signaling molecule through the guanylate cyclase system [6] in a manner similar to nitric oxide, but the proposal is still somewhat controversial. In the third step, biliverdin is formed from verdoheme with releasing Fe^{2+} in a reaction, which requires O_2 and reducing equivalents from NADPH cytochrome P450 reductase [7].

Two isoforms of HO, HO-1 and HO-2, are known. HO-1 (32 kDa) is highly expressed in spleen and liver, and is inducible by various substances including heme itself. It is involved in the response to oxidative stress [8]. In contrast, HO-2 (36 kDa) is constitutively expressed in brain, testis and vascular systems. It is suggested that the principal role of HO-2 is the production of CO as a neurotransmitter [8,9]. Rat HO-1, the topic of the present study, consists of 289 amino acids possessing a hydrophobic membrane binding domain at the C-terminus. We constructed an expression vector carrying a truncated HO-1 gene (Met1–Pro267) and succeeded in expressing a large amount of the water-soluble form of HO-1, which was fully as active as the membrane-bound form [10,11].

Recently the crystal structure of the human HO-1–heme complex was solved [12]. Here, we report the detailed structure of the rat HO-1 in complex with heme and discuss the heme oxygenase reaction on the basis of the structural comparison of the rat and human HO-1s.

2. Materials and methods

2.1. Preparation of heme–enzyme complexes

The truncated rat HO-1 was expressed and complexed with heme as previously described [10,11]. Selenomethionyl (SeMet) HO-1 was prepared in a similar way except for the following modifications. The methionine auxotrophic strain PLK-F′ (a gift from Toyobo) was transformed with the expression vector carrying the rat HO-1 gene, and was grown at 310 K for 75 h in an induction medium containing 10 mg/l L-selenomethionine (Sigma) and 40 mg/l of each of the other amino acids instead of casamino acids. Through the purification procedures, 5 mM dithiothreitol and 0.2 mM EDTA were added, and they were extensively removed by dialysis just prior to preparation of the complex with heme. For multi-wavelength anomalous dispersion (MAD) phase determination, we prepared two types of SeMet HO-1. One was a derivative in which all eight Met residues were replaced by SeMet residues (8SeMet HO-1). The other was a derivative that contained four SeMet residues (4SeMet HO-1); four of the eight codons of Met were mutated with Mutan-Express Km (Takara) at T157C, A277C, A463C and A571C, resulting in M51T, M93L, M155L and M191L, respectively. These residues are not conserved in rat HO-1, HO-2, human HO-1 or chicken HO-1. An unexpected additional mutation at F166S was found after construction of the plasmid.

2.2. Data collection and data processing

Heme–HO-1 complex crystal was grown at pH 8.5 as previously described [11]. Both of the SeMet HO-1s in complex with heme were crystallized under conditions similar to those for the native complex except for a decrease in the concentration of PEG 4000 from 27% (w/v) to 17% (w/v). 4SeMet HO-1–heme complex crystallized in needles with two molecules in an asymmetric unit. 8SeMet HO-1–heme complex crystallized in hexagonal rods which diffracted well at room temperature. We did not, however, collect full data for the latter crystal, because we were unable to find conditions suitable for cryostatic data collection.

For cryostatic data collection of native and 4SeMet HO-1, the crystals were transferred to the respective mother liquors, to which glycerol was added to 5% (w/v) for rat HO-1–heme complex crystal or to 6% (w/v) for 4SeMet HO-1–heme complex crystal. For 4SeMet HO-1–heme complex crystal, a slightly higher concentration of PEG 4000 in the mother liquor was used. Diffraction data for both crystals were collected at 100 K using synchrotron radiation at BL41XU of SPring-8 and the R-AXIS IV image plate system. The data were processed, merged and scaled with DENZO and SCALEPACK [13]. Measurement conditions and results are given in Table 1.

2.3. Model building and refinement

Our attempt to solve the crystal structure of the 4SeMet HO-1–heme complex by the MAD method was unsuccessful. The structure

*Corresponding author. Fax: (81)-6-6850 5425.
E-mail: fukuyama@bio.sci.osaka-u.ac.jp

[1] These authors contributed equally to this work.

PII: S0014-5793(00)01353-3

of the rat HO-1 heme complex was determined by the molecular replacement method with CNS [14]. The structure of human HO-1 (PDB code, 1QQ8), with 84% identity to the rat HO-1 in the amino acid sequence, was used for a search model in which heme, water and chloride ion were excluded. Since there are two possible space groups for the rat HO-1–heme crystal, $P4_32_12$ or $P4_12_12$, we tested the molecular replacement for both cases. After rigid body refinement, comparison of the electron density maps identified the space group of the crystal as $P4_32_12$. After protein atoms were refined by simulated annealing, we could clearly determine the position and orientation of the heme in the difference density map. The model of the heme was fitted to the density, and a few cycles of water picking and conjugate gradient minimization refinements were carried out. Finally, temperature factors were refined. All refinements are carried out using the reflections in the resolution range of 50.0–2.4 Å with CNS [14].

The structure of the 4SeMet HO-1–heme complex was determined in a similar way. Because the crystal of the 4SeMet HO-1–heme complex belongs to a different space group than that of the HO-1–heme complex, we calculated the cross-rotation and translation functions using the structure of the rat HO-1–heme complex, from which the heme and water molecules were excluded. This gave the orientation and position of one of two 4SeMet HO-1 complexes in an asymmetric unit. To determine the position of the other complex, we recalculated the translation function fixing the position of the 4SeMet HO-1 determined. As the space group of the crystal of the HO-1–heme complex is $P4_32_12$, we postulated the space group of this crystal to be $P4_3$ and this was confirmed by the subsequent refinement. The orientations of the heme groups were determined from the omit map after simulated annealing refinement. All refinements of 4SeMet HO-1 were carried out using the reflections in the 50.0–2.2 Å resolution range with CNS, where no restraint for non-crystallographic symmetry was applied to the model. The program O [15] was used for the adjustment and modeling of protein atoms, heme, and water molecules. The stereochemical checks of all models were carried out with PROCHECK [16]. Diffraction and refinement statistics are given in Table 1.

3. Results

3.1. Overall structure

The structure of the rat HO-1–heme complex has been refined to an *R* factor of 0.214 and a free *R* factor of 0.267 at 2.4 Å resolution. There is one molecule in an asymmetric unit. The final model contains a total of 1743 protein atoms, 43 heme atoms, and 60 water molecules. The structure of 4SeMet HO-1 has been refined to an *R* factor of 0.212 and a free *R* factor of 0.258 at 2.2 Å resolution. The final model contains a total of 3478 protein atoms, 86 heme atoms, and 143 water molecules. For both complexes, residues 10–223 could be built, whereas the first 9 and last 44 residues were disordered.

The two structures of the 4SeMet HO-1–heme complex in an asymmetric unit are identical to the structure of the rat HO-1–heme complex (Table 2A). The overall structure (Fig. 1) is mostly α-helical, and quite similar to the human HO-1–heme complex. The structure of the rat HO-1 has eight helices and nearly 65% of the resolved residues are in α-helices. The folding motif of HO-1 is distinct from the motifs of such heme proteins as globins and peroxidases.

3.2. Heme pocket

Heme is sandwiched between two helices, the proximal and distal helices. The δ-*meso* edge is exposed to the surface (Figs. 1 and 2). The proximal helix A (Fig. 1) consists of Leu13 to Gln29 including the proximal ligand of heme of His25 (Fig. 2). Previously, the proximal ligand of heme has been identified as His25 by spectroscopic methods [17,18]. The present X-ray analysis confirms the previous results.

The distal helix F (Fig. 1) consists of Leu129 to Met155 and bends at Leu141 and Ser142. According to spectroscopic studies [19–21], ferric heme iron in the rat HO-1 at pH 8.5 (our crystallization condition) should be low-spin with the distal ligand being OH^-. At the distal side of heme, we observed electron density which was 2.24 Å apart from the heme iron (Fig. 2), and we concluded that this electron density represents OH^-. Both Gly143N and Gly139O are close to OH^-. The distances from the hydroxyl oxygen to Gly143N and Gly139O are 2.60 and 2.93 Å, respectively (Fig. 2). In addition, the orientations of the amide group of Gly143 and the carbonyl group of Gly139 are appropriate to form hydrogen bonding to OH^-. Gly143 is conserved in all HOs previously known. In the rat HO-1, when Gly143 is replaced by other

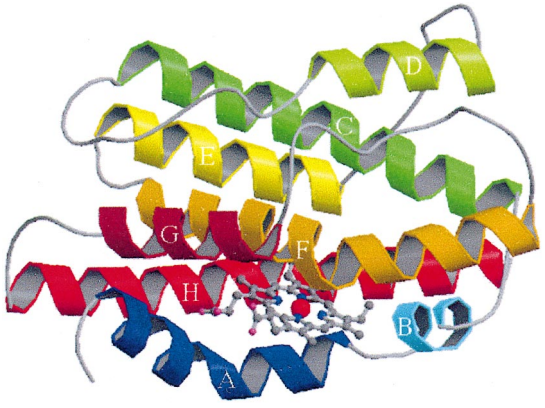

Fig. 1. Ribbon diagram of rat HO-1. Only backbone and heme are displayed. Helices were named A–H sequentially from the N-terminus to the C-terminus. A: Leu13–Glu29, colored blue; B: Glu32–Gln38, colored light blue; C: Arg44–Asn68, colored green; D: Arg86–Tyr97, colored yellow green; E: Pro109–Thr124, colored yellow; F: Leu129–Met155, colored orange; G: Pro175–Met186, colored brown; and H: Pro193–Thr222, colored red. The figure was prepared with MolScript [31] and Raster3D [32].

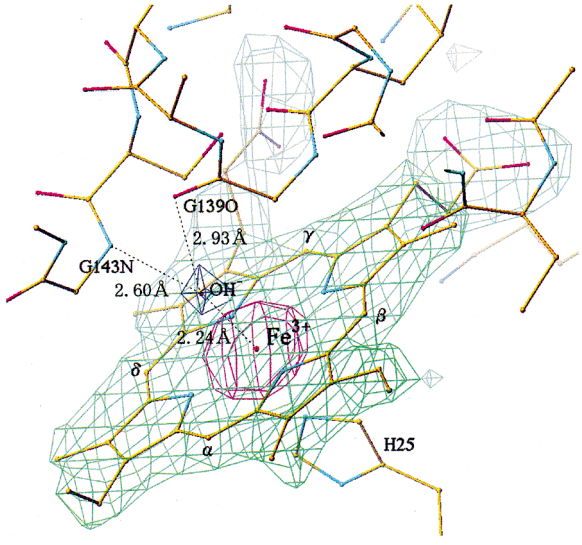

Fig. 2. Electron density map near heme. The omit map of the distal ligand of heme (purple) is overlaid on the $2F_o-F_c$ map of heme (green and magenta). View direction is from the distal side of heme. Green is over 3 σ level and magenta is over 10 σ. The electron density, displayed at the distal side of the heme plane, was assigned to be hydroxide on the basis of previous spectroscopic studies. The figure was prepared with Turbo-Frodo [33].

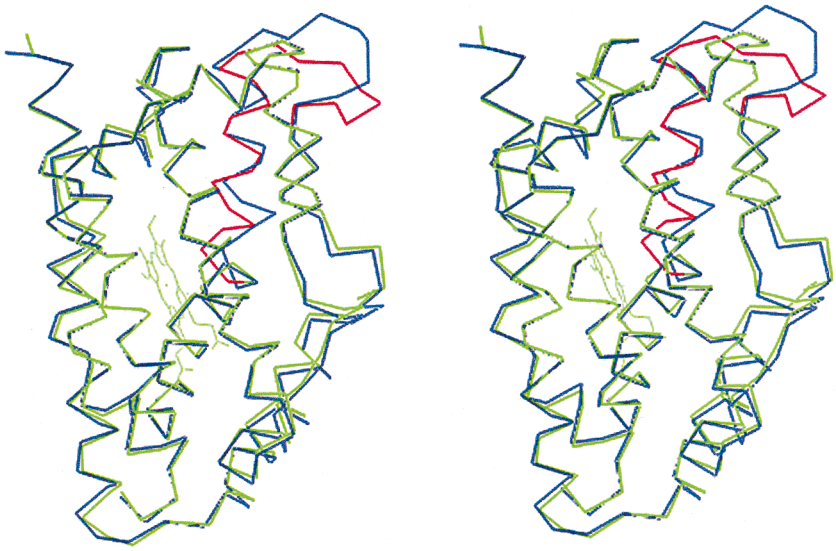

Fig. 3. Comparison of overall structures of rat and human HO-1–heme complexes. The figure is a stereo view showing rat HO-1 and human HO-1 opened form. Green stands for rat HO-1, blue for human HO-1 opened form, and red for rat HO-1 Leu141–Glu162. Superimpositions were carried out so as to minimize the square deviations of C_αs of all amino acids except for Leu141–Glu162. The figure was prepared with the program Turbo-Frodo.

amino acids, the space at the distal side of heme would become too narrow for heme to properly associate with HO, since the side chain of the replacing residue should be orientated to the heme.

In addition to His25, Lys18, Ala28, Glu29 in the proximal helix A and Met34 and Gln38 in helix B are in contact with the heme. In the distal helix F, Tyr134, Thr135, Arg136, Leu138 and Ser142 are in contact with the heme. In the other parts of the protein, Lys179, Arg183, Phe207, Asn210 and Phe214 are in contact with the heme. Lys18, Lys179 and Arg183 are clustered near propionate groups of the heme. This positively charged cluster should be important for the correct orientation of heme [22–24]. The correct orientation of heme is important for α-regiospecificity of the enzyme reaction. Further, there is a cavity surrounded by helix F on the distal side of the heme plane. The cavity restricts the orientation of the sixth ligand of heme towards α-*meso* carbon by steric interference. This is also important for α-regiospecificity.

4. Discussion

4.1. Comparison of the structures of rat and human HO-1s

Comparison of the structure of human HO-1 and that of rat HO-1 revealed that their overall structures are similar except for the segment from Leu141 to Glu162 (Fig. 3). The rmsd between C_α atoms of these amino acids is given in Table 2B.

Within the heme pocket, the position of Gly143 in the rat and human HO-1s differs markedly (Fig. 4). In the case of globins and peroxidases, a polar side chain of distal amino acids such as histidine is considered to stabilize an oxygen ligand. In the case of human HO-1, however, no polar side chain is present. In the human HO-1, Schuller et al. [12] suggested that the carbonyl oxygen of Gly139 and nitrogen of Gly143 are candidates for the distal polar groups. They also described that human HO-1 has two conformations, opened and closed forms. In the closed form, a distal helix F is draped across the heme, and this bent helix is considered to prevent

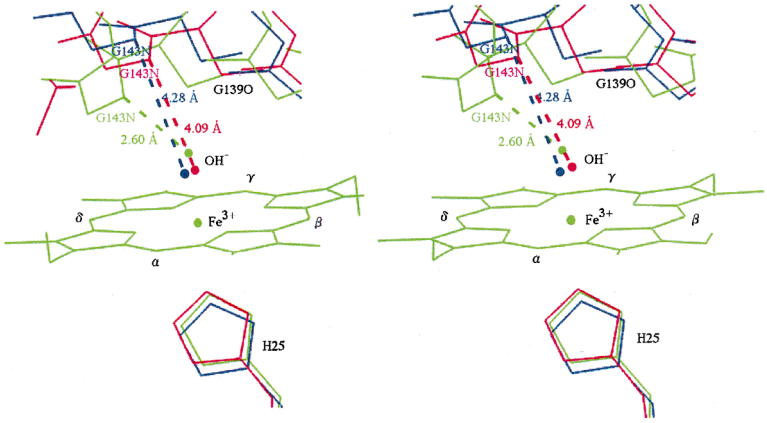

Fig. 4. Stereo view of the structures of rat and human HO-1s near the heme. Green stands for rat HO-1, blue for human HO-1 opened form and red for human HO-1 closed form. Superimpositions were carried out so as to minimize the sums of the square deviations of C_αs. The figure was prepared with Turbo-Frodo and LSQMAN [34].

Table 1
Summary of crystallographic statistics

	HO-1–heme complex	4SeMet HO-1–heme complex
Measurement condition		
Wavelength (Å)	0.890	0.9793
Distance between crystal and IP (mm)	390	300
Oscillation angle (deg)	2.5	2.5
Measurement angle (deg)	95	75
Crystallographic data		
Crystal system	tetragonal	
Space group	$P4_32_12$	$P4_3$
Unit cell dimensions (Å)	$a=b=56.1$ $c=184.0$	$a=b=54.8$ $c=187.4$
Molecules in asymmetric unit	1	2
Diffraction statistics		
Resolution (Å)	2.4	2.2
Mosaicity (deg)	0.8	0.2
No. of observations	69 033	69 625
No. of unique reflections	12 148	26 625
Completeness(%)	98.7 (95.5)[c]	95.1 (89.8)[c]
Mean I/σ	16.7	7.3
R_{sym} [a]	0.063 (0.174)[c]	0.087 (0.227)[c]
Refinement statistics		
R/R_{free} [b]	0.214/0.267	0.212/0.257
Rmsd bond lengths (Å)	0.006	0.006
Rmsd angles (deg)	1.09	1.14
No. of water molecules	60	143
Ramachandran angles		
Most favored (%)	91.1	91.6
Additional allowed (%)	8.9	8.1
Generously allowed (%)	0.0	0.3

[a] $R_{sym}=\Sigma\Sigma_j|I_j-\langle I\rangle|/\Sigma|\langle I\rangle|$, where I_j is the intensity measurement for reflection j and $\langle I\rangle$ is the mean intensity for multiple recorded reflections.
[b] $R=\Sigma||F_{obs}|-|F_{calc}||/\Sigma|F_{obs}|$. R_{free} is R calculated for 5% of the dataset not including refinements.
[c] Values in parentheses are for the outermost shell.

the access of the iron-bound peroxide to the other *meso* carbons except for the α-*meso* carbon. The distance between Gly143N and the water ligand is 4.09 Å in the closed form and 4.28 Å in the opened form. The distance between the Gly139O and the water ligand is 3.27 Å in the closed form and 3.25 Å in the opened form (Fig. 4).

In the rat HO-1, the distance between Gly143N and hydroxide is shorter than that in the human HO-1 (Fig. 4). From the orientation of the amide group of Gly143 and the distance between Gly143N and the hydroxide (2.60 Å), it is fully conceivable that Gly143N can be hydrogen-bonded to the hydroxide. On the other hand, hydrogen bond formation between the hydroxide and Gly139O is also possible based on the distance between them (2.93 Å).

The amino acid sequence in the segment from Leu141 to Glu162 is identical in both of the rat and the human HO-1s except for Met155 and Ala156 in the rat HO-1 and Leu155 and Asp156 in the human HO-1, and the overall identity of amino acid sequence between the rat and human HO-1s is 84%. Therefore, the structural difference of the segment between two HO-1s cannot be attributed to the slight difference in amino acid sequences due to species.

4.2. Conformation change

In the distal helix F after the bending point at Leu141 and Ser142, the temperature factors of the human HO-1 closed form are higher than those of the human HO-1 opened form and rat HO-1 (data not shown). Also the dihedral angles of Leu141 and Ser142 are markedly different between the rat and human HO-1s. These findings suggest that the structure of helix F after the bending point is flexible and that the bending point plays a role as a hinge to produce the flexibility.

Table 2
The rmsd of C_αs among rat HO-1, human HO-1 and 4SeMet HO-1

A: Rat HO-1 versus 4SeMet HO-1

	Rat HO-1	4SeMet HO-1A	4SeMet HO-1B
Rat HO-1	–	0.435	0.412
4SeMet HO-1A	0.377	–	0.246
4SeMet HO-1B	0.409	0.222	–

B: Rat HO-1 versus human HO-1

	Rat HO-1	Human HO-1 opened form	Human HO-1 closed form
Rat HO-1	–	1.051	1.043
Human HO-1 opened form	1.788	–	0.499
Human HO-1 closed form	1.668	0.526	–

A: rmsd of C_αs between the rat and 4SeMet HO-1s. There are two molecules (A and B) in an asymmetric unit of the 4SeMet HO-1 crystal. B: rmsd of C_αs between the rat and human HO-1. The upper right and lower left figures of each pair of diagonal terms represent the rmsd of C_αs of all amino acids and that of amino acids in Leu141–Glu162, respectively.

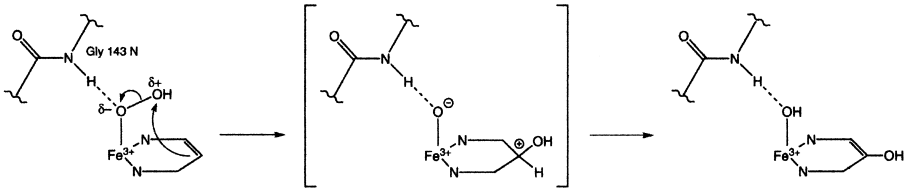

Fig. 5. Possible mechanism of the electrophilic addition of the ferric peroxide to the porphyrin ring.

Further, the structure from Ala156 to Glu162, a loop linked from helix F, also differs between the rat and human HO-1s (Fig. 3). Because the dihedral angles of each residue in the region are different between rat and human HO-1s (data not shown), the region of Ala156 to Glu162 differs in its conformation. It appears as though the region provides a cushion for minimizing the change of the overall structure when the conformation of helix F changes.

The structural difference observed between the rat and human HO-1s would be due to the different pHs when they were crystallized. The rat HO-1 was crystallized at pH 8.5, the human HO-1 at pH 7.5 [25]. Spectroscopic studies of the HO-1–heme complex suggested a pH-dependent spin shift of ferric heme iron from high to low spin, accompanying replacement of the sixth ligand, water, with hydroxide ($pK_a \approx 7.6$) [4,19–21,26]. Although these spectroscopic studies were carried out with rat HO-1, the spin shift should also take place in the human HO-1, because the amino acid sequences and the structures of the rat and human HO-1s are similar. Taking this pH shift and the difference in conformation into account, the structure of the human HO-1 opened form is considered to represent the conformation when the heme iron is high-spin, while the structure of the rat HO-1 represents the conformation when the heme iron is low-spin. Further, the structure of the human HO-1 closed form is regarded as an intermediate between these conformations. It will be necessary to determine the crystal structure below pH 6.5 to clarify this.

4.3. Implications of the structure of HO-1–heme complex for the HO reaction

The HO reaction is conspicuous compared to other heme enzyme reactions such as those in peroxidases and cytochrome P450 in some respects. For the first α-*meso* carbon hydroxylation, it utilizes a peroxy-type oxygen instead of the compound I-type oxyferryl intermediate that is believed to be the active species in P450 and peroxidase reactions [27,28]. Further, Ortiz de Montellano and coworkers, using ethyl hydroperoxide as cosubstrate, ruled out a mechanism in which the terminal oxygen of a ferric peroxo anion (Fe^{III}–OO^-) is added as a nucleophile to the porphyrin, but proposed instead the mechanism of electrophilic addition of the ferric peroxide (Fe^{III}–OOH) terminal oxygen to the porphyrin [22,29]. As shown in the rat HO-1 structure, Gly143N can be hydrogen-bonded to the oxygen atom of ferric hydroxide. If Gly143N is also hydrogen-bonded to the proximal oxygen of the ferric peroxide as a proton donor, it should stabilize the negative charge of the proximal oxygen and assist the electrophilic addition of the terminal oxygen to the porphyrin, along with a heterolytic O–O bond cleavage of the ferric peroxide (Fig. 5).

Resonance Raman studies [19,20,30] have indicated that dioxygen bound to a ferrous iron is highly bent toward α-*meso* carbon, supporting the α-regioselectivity in the HO reaction. The crystal structure of the rat HO-1 also indicates that steric control is critical for the α-regiospecificity. The distal helix F drapes across the entire width of heme, preventing the access of ferric hydroperoxide to the β-, γ- and δ-*meso* carbons.

Recently we reported that the ferric α-hydroxyheme bound to HO-1 can be converted to the ferrous verdoheme by dioxygen alone without added reducing equivalents [5]. The reactive molecular form of the α-hydroxyheme responsible for the conversion to verdoheme is the ferrous π-neutral radical form, the formation of which is greatly accelerated by the presence of the sixth ligand that keeps the heme iron low-spin. In this reaction, dioxygen directly attacks the radical at the heme edge without oxygenation of iron. ESR analysis of the resultant verdoheme suggested that the heme iron is low-spin and possesses hydroxide as a sixth ligand. Hence it seems to be advantageous for heme to be kept low-spin during the conversion of α-hydroxyheme to verdoheme. In the first α-hydroxylation of heme, the proximal oxygen of the ferric peroxide is left as hydroxide at the sixth coordination site of the heme. If Gly143N is able to stabilize the hydroxide through hydrogen bonding and the hydroxide is able to keep the heme iron low-spin, the conversion of α-hydroxyheme to verdoheme would become feasible.

The structure of the HO-1–heme complex is unique in that the proximal ligand is a neutral His [17,18] and Gly139 and 143 are located as the closest distal residues rather than any polar residues. Also unique is the HO reaction in that the hydroxylation of heme takes place with a ferric peroxide. The role of the two glycine residues, especially Gly143, in the first hydroxylation and in the downstream reactions is now only speculative. In this context, determination of the crystal structures of the heme–HO-1 complex at acidic pHs as well as those of the HO-1 complex with the heme degradation intermediates is awaited with much interest.

The coordinates of both complexes have been deposited to the Protein Data Bank with accession codes 1DVE and 1DVG.

Acknowledgements: We thank Drs. Masahide Kawamoto of JASRI and Nobuo Kamiya of RIKEN for their valuable help with data collection using synchrotron radiation of BL41XU, SPring-8. This work was supported in part by Grants-in-Aid for Scientific Research on Priority Areas (Molecular Biometallics and Biological Machinery) to K.F. (No. 10129219) and to M.N. (Nos. 1116227 and 11169240) from the Ministry of Education, Science, Sports, and Culture, Japan.

References

[1] Yoshida, T., Noguchi, M., Kikuchi, G. and Sano, S. (1981) J. Biochem. (Tokyo) 90, 125–131.
[2] Yoshinaga, T., Suto, Y. and Sano, S. (1990) Biochem. J. 270, 659–664.

[3] Liu, Y., Moenne-Loccoz, P., Loehr, T.M. and Ortiz de Montellano, P.R. (1997) J. Biol. Chem. 272, 6906–6917.
[4] Matera, K.M., Rousseau, D.L., Yoshida, T. and Ikeda-Saito, M. (1996) J. Biol. Chem. 271, 6618–6624.
[5] Sakamoto, H., Omata, Y., Palmer, G. and Noguchi, M. (1999) J. Biol. Chem. 274, 18196–18200.
[6] Maines, M.D. (1997) Annu. Rev. Pharmacol. Toxicol. 37, 517–554.
[7] Yoshida, T. and Kikuchi, G. (1978) J. Biol. Chem. 253, 4230–4236.
[8] Prabhakar, N.R. (1998) Respir. Physiol. 114, 57–64.
[9] Prabhakar, N.R. (1999) Respir. Physiol. 115, 161–168.
[10] Hidaka, T., Omata, Y. and Noguchi, M. (1996) Kurume Med. J. 43 (4), 313–324.
[11] Omata, Y., Asada, S., Sakamoto, H., Fukuyama, K. and Noguchi, M. (1998) Acta Crystallogr. D 54, 1017–1019.
[12] Schuller, D.J., Wilks, A., Ortiz de Montellano, P.R. and Poulos, T.L. (1999) Nature Struct. Biol. 6, 860–867.
[13] Otwinowski, Z. and Minor, W. (1997) Methods Enzymol. 276, 472–494.
[14] Brunger, A.T., Adams, P.D., Clore, G.M., DeLano, W.L., Gros, P., Grosse-Kunstleve, R.W., Jiang, J.S., Kuszewski, J., Nilges, N., Pannu, N.S., Read, R.J., Rice, L.M., Simonson, T. and Warren, G.L. (1998) Acta Crystallogr. D 53, 905–921.
[15] Jones, T.A., Zou, J.Y., Cowan, S.W. and Kieldgaard, M. (1991) Acta Crystallogr. A 47, 110–119.
[16] Laskowski, R.A., MacArthur, M.W., Moss, D.S. and Thornton, J.M. (1993) J. Appl. Crystallogr. 26, 283.
[17] Ito-Maki, M., Ishikawa, K., Matera, K.M., Sato, M., Ikeda-Saito, M. and Yoshida, T. (1995) Arch. Biochem. Biophys. 317, 253–258.
[18] Sun, J., Loehr, T.M., Wilks, A. and Ortiz de Montellano, P.R. (1994) Biochemistry 33, 13734–13740.
[19] Takahashi, S., Wang, J., Rousseau, D.L., Ishikawa, K., Yoshida, T., Takeuchi, N. and Ikeda-Saito, M. (1994) Biochemistry 33, 5531–5538.
[20] Takahashi, S., Wang, J., Rousseau, D.L., Ishikawa, K., Yoshida, T., Jenette, R.H. and Ikeda-Saito, M. (1994) J. Biol. Chem. 268, 1010–1014.
[21] Hawkins, B.K., Wilks, A., Powers, L.S., Ortiz de Montellano, P.R. and Dawson, J.H. (1996) Biochim. Biophys. Acta 1295, 165–173.
[22] Wilks, A., Torpey, J. and Ortiz de Montellano, P.R. (1994) J. Biol. Chem. 269, 29553–29556.
[23] Torpey, J. and Ortiz de Montellano, P.R. (1996) J. Biol. Chem. 271, 26067–26073.
[24] Torpey, J. and Ortiz de Montellano, P.R. (1997) J. Biol. Chem. 272, 22008–22014.
[25] Schuller, D.J., Wilks, A., Ortiz de Montellano, P.R. and Poulos, T.L. (1998) Protein Sci. 7, 1836–1838.
[26] Sun, J., Wilks, A., Ortiz de Montellano, P.R. and Loehr, T.M. (1993) Biochemistry 32, 14151–14157.
[27] Brown, S.B., Chabot, A.A., Enderby, E.A. and North, A.C.T. (1981) Nature 289, 93–95.
[28] Noguchi, M., Yoshida, T. and Kikuchi, G. (1983) J. Biochem. (Tokyo) 93, 1027–1036.
[29] Wilks, A. and Ortiz de Montellano, P.R. (1993) J. Biol. Chem. 268, 22357–22362.
[30] Takahashi, S., Ishikawa, K., Takeuchi, N., Ikeda-Saito, M., Yoshida, T. and Rousseau, D.L. (1995) J. Am. Chem. Soc. 117, 6002–6006.
[31] Kraulis, P.J. (1991) J. Appl. Crystallogr. 24, 946–950.
[32] Merritt, E.A. and Bacon, D.J. (1997) Methods Enzymol. 277, 505–524.
[33] Roussel, A. and Cambillau, C. (1989) in: Silicon Graphics Germany Partner, Directory, pp. 77–78, Silicon Graphics, Mountain View, CA.
[34] Kleywegt, G.J. and Jones, T.A. (1994) CCP4/ESF-EACBM Newslett. Protein Crystallogr. 31, 9–14.